Engineering 27 (2023) 96–105

Contents lists available at ScienceDirect

Engineering

journal homepage: www.elsevier.com/locate/eng

Research
Smart Process Manufacturing toward Carbon Neutrality—Article

Multi-Objective Adaptive Optimization Model Predictive Control: Decreasing Carbon Emissions from a Zinc Oxide Rotary Kiln

Ke Wei, Keke Huang *, Chunhua Yang, Weihua Gui

School of Automation, Central South University, Changsha 410083, China

ARTICLE INFO

Article history:
Received 23 August 2022
Revised 4 November 2022
Accepted 14 January 2023
Available online 22 July 2023

Keywords:
Zinc oxide rotary kiln
Model reduction
Sparse identification
Real-time optimization
Model predictive control
Process control

ABSTRACT

The zinc oxide rotary kiln, as an essential piece of equipment in the zinc smelting industrial process, is presenting new challenges in process control. China's strategy of achieving a carbon peak and carbon neutrality is putting new demands on the industry, including green production and the use of fewer resources; thus, traditional stability control is no longer suitable for multi-objective control tasks. Although researchers have revealed the principle of the rotary kiln and set up computational fluid dynamics (CFD) simulation models to study its dynamics, these models cannot be directly applied to process control due to their high computational complexity. To address these issues, this paper proposes a multi-objective adaptive optimization model predictive control (MAO-MPC) method based on sparse identification. More specifically, with a large amount of data collected from a CFD model, a sparse regression problem is first formulated and solved to obtain a reduction model. Then, a two-layered control framework including real-time optimization (RTO) and model predictive control (MPC) is designed. In the RTO layer, an optimization problem with the goal of achieving optimal operation performance and the lowest possible resource consumption is set up. By solving the optimization problem in real time, a suitable setting value is sent to the MPC layer to ensure that the zinc oxide rotary kiln always functions in an optimal state. Our experiments show the strength and reliability of the proposed method, which reduces the usage of coal while maintaining high profits.

© 2023 THE AUTHORS. Published by Elsevier LTD on behalf of Chinese Academy of Engineering and Higher Education Press Limited Company. This is an open access article under the CC BY-NC-ND license (http://creativecommons.org/licenses/by-nc-nd/4.0/).

1. Introduction

Given the urgent necessity of achieving a carbon peak and carbon neutrality, the manufacturing and recycling of zinc oxide in the zinc smelting industry are presenting new challenges, due to the high energy usage and environmental pollution of these processes [1–4]. In general, to produce 1 t of zinc, a well-equipped plant consumes about 460 kg of coal, with emissions equivalent to more than 3 t of carbon dioxide (CO_2) [5]. It is obvious that the more coal is burned, the more greenhouse gases will be emitted; thus, an efficient way to achieve carbon neutrality is to cut coal consumption. As an essential piece of equipment in the zinc smelting industry, the rotary kiln consumes the greatest proportion of coal as an energy supply to maintain a suitable reaction atmosphere for recycling zinc oxide, thereby producing greenhouse gases with a great impact on the environment [6]. More importantly, a rotary kiln is a typical distributed parameter system [7], which makes it difficult to obtain all the sensor information to evaluate its reaction atmosphere, leading to the emission of polluting gases such as carbon monoxide (CO). Therefore, it is necessary to study the characteristics of the zinc oxide rotary kiln in detail to enable its performance enhancement [8].

Over the decades, in order to figure out the principle of the rotary kiln, modeling research has accumulated a number of works that lay a foundation for bringing the rotary kiln from the physical world into digital space. For example, Boateng and Barr [9] came up with a thermal model for the rotary kiln that includes heat transfer within the bed, and Wang et al. [10] proposed a mathematical model of a rotary kiln that not only considers the reaction mechanisms but also reduces the computation complexity. Recently, in order to optimize the operation performance of the rotary kiln, researchers have gradually come to focus on establishing thermal models for the rotary kiln, since the distribution of temperature has a major impact on the reaction atmosphere [11,12]. Meanwhile, with the development of computing power, new computational fluid dynamics (CFD) technology has been

* Corresponding author.
E-mail address: huangkeke@csu.edu.cn (K. Huang).

https://doi.org/10.1016/j.eng.2023.01.017
2095-8099/© 2023 THE AUTHORS. Published by Elsevier LTD on behalf of Chinese Academy of Engineering and Higher Education Press Limited Company.
This is an open access article under the CC BY-NC-ND license (http://creativecommons.org/licenses/by-nc-nd/4.0/).

widely introduced into large-scale system modeling. Witt et al. [13] built up a CFD simulation of a rotary kiln that includes granular flow and heat transfer. With the help of a CFD model, Ditaranto and Bakken [14] managed to improve the rotary kiln operating conditions to achieve higher combustion efficiency.

Although academia has made great progress in rotary kiln modeling, the works in the literature cannot be directly applied to industrial sites, since a CFD simulation requires high computing resources and does not satisfy the demands of real-time decision-making in practice. Therefore, most CFD simulations are used to guide workers in determining the optimal design parameters of a rotary kiln before construction. Researchers have attempted to explore the balance between the accuracy of the simulation model and real-time computing demand, leading to the development of reduced-order models (ROMs) [15]. The purpose of a ROM is to significantly reduce computational complexity while maintaining the model accuracy compared with the original CFD simulation. Two widely used approaches to obtain ROMs include projection-based model reduction [16–18] and subspace model identification [19–21]. In the projection-based method, a vector field is decomposed into a set of modes and the system operators are projected onto a low-dimensional subspace to reduce the computational complexity. In subspace model identification, the original model is transferred into a multivariable linear model based on state-space models. These methods have been demonstrated to be effective in several nonlinear systems. Nevertheless, they still have a drawback: Once reduction models are found, the physical meaning of the states and the structure of the original system are completely lost, which is not suitable for further process monitoring and control.

To address the abovementioned limitations, innovative sparse identification methods inspired by compressive sensing and sparse regression have been put forward [22–24]. In sparse identification, the original data—without additional transformation—are applied to formulate a basis function library. By performing nonlinear sparse regression on a large library of potential candidate functions, the fewest terms that most accurately represent the data are found. Kaiser et al. [25] applied sparse identification to predict nonlinear dynamics for model predictive control (MPC) with low data. Bhadriraju et al. [26] proposed an operable adaptive sparse identification combined with deep neural networks to deal with plant-model mismatch, and Li et al. [27] considered the impact of noise on sparse identification and put forward a robust sparse identification method. These works provide new methods of obtaining ROMs and demonstrate the promising prospects of sparse identification.

Since a ROM can save on computing resources and satisfy the demands of real-time computing, it is possible to use this method to improve the performance of a zinc oxide rotary kiln with the help of advanced control strategies. MPC is an efficient control method that is widely applied in industrial processes. It includes three fundamental elements: a predictive model of the controlled system, a reference trajectory, and an optimal controller obtained via rolling optimization [28–30]. In research on rotary kilns, most researchers focus on how to realize temperature stability control in the reaction zone [31,32]. For example, Stadler et al. [33] and Machalek and Powell [34] combined a first-principles model with an MPC framework to optimize operation performance of reaction zone accordingly. However, with the urgent necessity of achieving a carbon peak and carbon neutrality, relying on stability control alone cannot ensure optimal economic benefits. If the given setting value is not reasonable, even if most of the monitoring indicators remain stable, the reaction atmosphere will worsen, resulting in the emission of more greenhouse or polluting gases. To satisfy the new demand for optimal control, a new two-layered control framework including real-time optimization (RTO) and MPC has been developed [35,36]. The RTO-MPC framework can not only keep a controlled plant stable but also determine the optimal-setting value based on economic indicators, thereby providing a new perspective for the optimal control of a rotary kiln.

Inspired by the development of modeling and optimal control in complex industrial processes and the new production demands for zinc oxide rotary kilns, we propose a multi-objective adaptive optimization model predictive control (MAO-MPC) method based on a first-principles model and sparse identification. First, we establish a dynamical CFD model of a zinc oxide rotary kiln based on the law of energy conservation. Then, since the CFD model is too complex to calculate in real time, we put forward a sparse identification-based model-reduction method. More specifically, a function library is formulated with the help of original data obtained from the CFD model. By solving a sparse regression problem, the ROM is determined. Finally, a two-layered control framework including RTO and MPC is proposed. In the RTO layer, an optimization problem with the goal of achieving optimal process operation performance is set up. By solving the optimization problem in real time, a suitable setting value can be sent to the MPC layer to ensure that the zinc oxide rotary kiln is always working in an optimal state. Several experiments demonstrate the superiority of the proposed method in improving the control effect. In summary, the main contributions of this paper are threefold.

(1) A sparse identification-based ROM is proposed to overcome the high computational complexity of the traditional dynamical CFD model, making it possible to obtain the dynamics of a zinc oxide rotary kiln in real time.

(2) An optimization problem is formulated in the RTO layer that takes the economic performance of the process and the demand to reduce greenhouse gas emissions into consideration to determine the optimal-setting value for process control.

(3) The MAO-MPC method is proposed for an industrial zinc oxide rotary kiln; the proposed method not only maintains the kiln working efficiently but also decreases coal consumption.

The rest of this paper is organized as follows: In Section 2, a brief introduction to the zinc oxide rotary kiln process is formulated and a first-principles model is established. Details of the proposed ROM based on sparse identification and the MAO-MPC method are presented in Section 3, while Section 4 gives an analysis and discussion of the experimental results. Section 5 provides the concluding remarks of this paper.

2. Process description

This section first presents a brief introduction to the zinc oxide rotary kiln process. Then, a dynamical CFD model of a zinc oxide rotary kiln is established based on the law of energy conservation. This model generates the data that becomes the foundation of the proposed method.

2.1. Zinc oxide rotary kiln process

The zinc oxide rotary kiln is an essential piece of equipment in the zinc smelting industrial process that largely determines whether the raw production materials are fully utilized. A production flow chart of the zinc smelting process is provided in Fig. 1. The raw materials are directly sent to the roaster to produce zinc concentrate. Through a series of ionic and electrochemical reactions in the hydrometallurgy process, a pure zinc product is obtained. During the hydrometallurgy process, the leaching step dissolves the zinc element in the raw materials into a solution, while other elements such as lead and silver remain as byproducts in a solid called the leaching residue. However, in practice in the production process, some zinc oxide is mixed into the leaching residue before further reactions occur. Therefore, a rotary kiln is

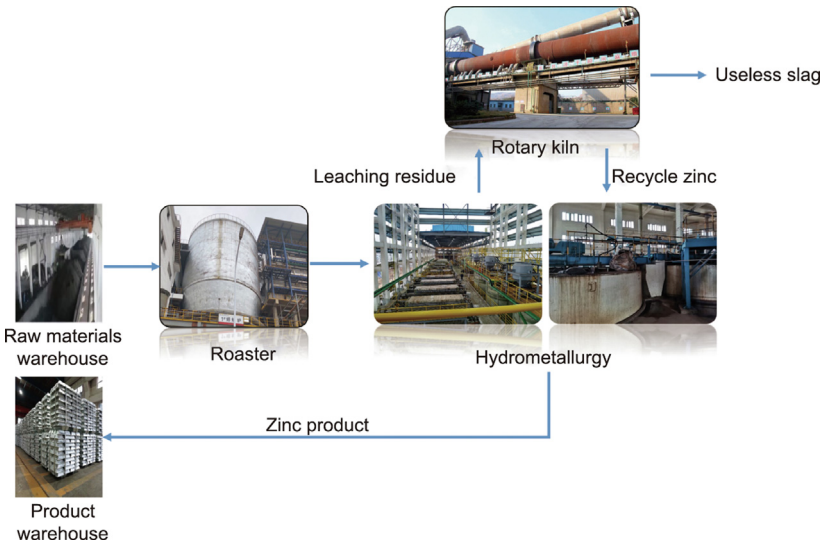

Fig. 1. The zinc smelting industrial process.

applied to avoid wasting zinc oxide. More specifically, when the leaching residue is sent to the rotary kiln, high temperature calcination and redox reactions are used to separate the zinc oxide from the leaching residue. The zinc oxide is then sent back to the hydrometallurgy process, increasing resource utilization.

The structure of a zinc oxide rotary kiln is shown in Fig. 2. According to the temperature distribution, the inside of a rotary kiln is divided into several zones: the dry zone, preheat zone, reaction zone, and cooling zone. Since the kiln body is on an incline and is constantly rotating, the materials inside the kiln slowly move from the top (the tail) to the bottom (the head) while undergoing a circular motion along the kiln wall. When the leaching residue mixed with coal is fed into the rotary kiln at the tail, it passes through the dry zone and preheat zone, which remove moisture and prepare the residue for subsequent reactions. Redox reactions take place in the reaction zone, yielding pure zinc gas with a temperature of up to 1000–1200 °C. A large amount of air is blown to oxidize the pure zinc gas to zinc oxide gas and blow it back out of the tail of the rotary kiln. The reaction atmosphere in the reaction zone determines whether the rotary kiln performs well or not. As the temperature distribution inside the kiln has a strong relationship with the reaction atmosphere, it is necessary to figure out how temperature varies along the axis of the kiln.

2.2. Modeling the kiln temperature distribution along the axis

The dynamic mathematical model of the temperature distribution along the kiln axis is based on energy balance equations for three phases within the rotary kiln: the freeboard gas, solid bed, and wall. Fig. 3 shows a cross-section of the rotary kiln, where T_g is the freeboard gas temperature, T_s represents the solid bed temperature, T_w denotes the wall temperature, and T_o stands for the temperature of the environment.

To make the model as simple as possible while maintaining the essential dynamics, the following assumptions have been made [10,37]:

- The axial linear velocity changes of both the solid and the gas are negligible.
- There is neither solid nor gas axial mixing. The two phases are considered to be a plug flow model. Solid drag by the gas is negligible.
- The heat transfer and specific heat coefficients are constant.
- The mass changes of the solid and the gas in the axial direction caused by the reaction are negligible.
- Coal combustion is the main heat source, and the reaction heat is negligible.
- The wall has no ability to store or consume any energy; thus, its net energy is zero.

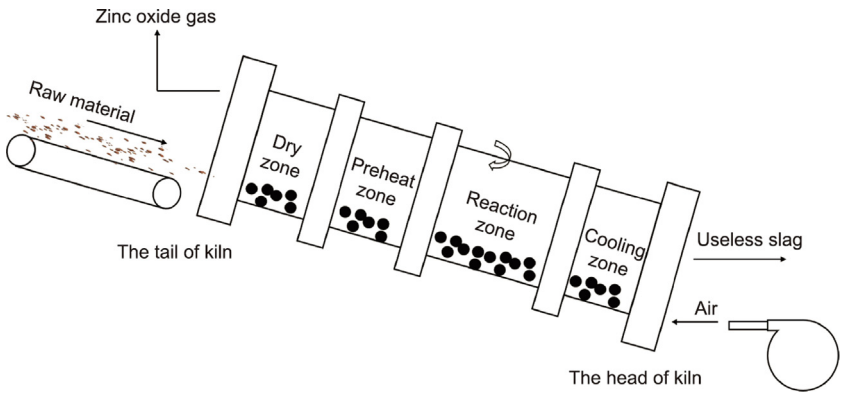

Fig. 2. Schematic of a zinc oxide rotary kiln.

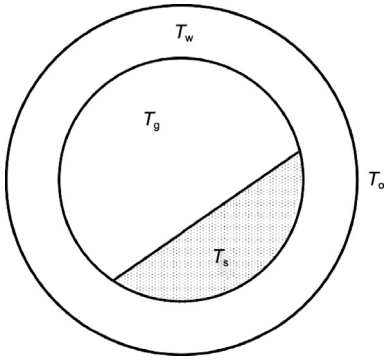

Fig. 3. Cross-section of a rotary kiln.

Based on the above assumptions, the following mathematical expressions of the dynamic model can be formulated [10–12]:

Gas phase:

$$c_g m_g \frac{\partial T_g}{\partial t} = -v_g c_g m_g \frac{\partial T_g}{\partial x} + \psi_{sg} A_{sg}(T_s - T_g) + \psi_{wg} A_{wg}(T_w - T_g) + \sigma \varepsilon_s \varepsilon_g A_{sg}\left(T_s^4 - T_g^4\right) + \sigma \varepsilon_w \varepsilon_g A_{wg}\left(T_w^4 - T_g^4\right) + Q_c^i \quad (1)$$

Solid phase:

$$c_s m_s \frac{\partial T_s}{\partial t} = -v_s c_s m_s \frac{\partial T_s}{\partial x} + \psi_{sg} A_{sg}(T_g - T_s) + \psi_{ws} A_{ws}(T_w - T_s) + \sigma \varepsilon_s \varepsilon_g A_{sg}\left(T_g^4 - T_s^4\right) + \sigma \varepsilon_w \varepsilon_s A_{ws}\left(T_w^4 - T_s^4\right) \quad (2)$$

Wall phase:

$$c_w m_w \frac{\partial T_w}{\partial t} = \psi_{wg} A_{wg}(T_g - T_w) + \psi_{ws} A_{ws}(T_w - T_s) + \sigma \varepsilon_w \varepsilon_g A_{wg}\left(T_g^4 - T_w^4\right) + \sigma \varepsilon_w \varepsilon_s A_{ws}\left(T_s^4 - T_w^4\right) + \psi_{wo} A_{wo}(T_o - T_w) \quad (3)$$

where x and t are space and time domains, respectively; v_g and v_s represent the movement speed of the gas and the solid, respectively; and Q_c^i in Eq. (1) is the heat generated by coal combustion at position i, whose expression can be formulated as follows [37]:

$$Q_c^i = m_{coal} Q_{net}\left(e^{-3.912 L_{i+1}/L_f^2} - e^{-3.912 L_i/L_f^2}\right) \quad (4)$$

where m_{coal} represents the mass of coal; Q_{net} is the heat of combustion of coal, which is equal to 29 MJ·kg^{-1}; L_f stands for the length of the flame; and L_i is the distance between the flame and position i inside the rotary kiln. The physical meanings of all the parameters are provided in Table 1, while Table 2 lists the values of these parameters, which are mainly determined according to Ref. [38] and a design drawing of a rotary kiln obtained from an industrial site. With the help of CFD simulation software such as COMSOL, the solution of the dynamical model above can be found, laying a foundation for optimal control of the rotary kiln reaction atmosphere.

3. Proposed method

In this section, the proposed MAO-MPC method based on sparse identification is introduced in detail, with the aim of improving the performance of a rotary kiln.

3.1. Motivation

With the dynamical CFD model, a large amount of data can be collected to analyze and monitor the operation status of the rotary kiln. However, when it comes to improving the reaction atmosphere through an advanced control strategy, the CFD model cannot be directly applied due to its high computational complexity, which decreases its practical application value. On the other hand, with the increasing need to contribute to the goal of achieving a carbon peak and carbon neutrality, traditional stability control is not suitable for a multi-objective case with the requirements of reducing environmental pollution and resource consumption while ensuring high-level production efficiency. Thus, to further improve the performance of the rotary kiln, we propose an MAO-MPC method based on sparse identification. Our proposed method has two essential parts: a model reduction and a two-layer control framework including RTO layer and an MPC layer. Inspired by sparse regression and its powerful capacity for representation, sparse identification is applied to reduce the model order and computational complexity while retaining the key dynamics in the CFD model. An optimization problem is designed in the RTO layer with the goal of achieving optimal process operation performance, which provides an optimal-setting value to ensure that the rotary kiln is always working in an optimal state.

Table 1
List of parameters in the CFD model.

Parameter	Physical meaning
c_g	Specific heat of gas
c_s	Specific heat of solid
c_w	Specific heat of kiln wall
m_g	Mass of gas
m_s	Mass of solid
m_w	Mass of kiln wall
A_{sg}	Surface area between gas and solid
A_{wg}	Surface area between gas and wall
A_{ws}	Surface area between solid and wall
A_{wo}	Surface area between environment and wall
ψ_{sg}	Convection coefficient between gas and solid
ψ_{wg}	Convection coefficient between gas and wall
ψ_{ws}	Convection coefficient between solid and wall
ψ_{wo}	Convection coefficient between environment and wall
σ	Coefficient of radiation
ε_g	Emissivity of gas
ε_s	Emissivity of solid
ε_w	Emissivity of wall

Table 2
Values of the parameters in the CFD model.

Parameter term	Value
$c_g m_g$	450.00
$c_s m_s$	550.00
$c_m m_m$	55.00
$\psi_{sg} A_{sg}$	74.50
$\psi_{wg} A_{wg}$	5.10
$\psi_{ws} A_{ws}$	2.50
$\psi_{wo} A_{wo}$	119.30
$\sigma \varepsilon_s \varepsilon_g A_{sg}$	5.04×10^{-8}
$\sigma \varepsilon_w \varepsilon_s A_{ws}$	5.22×10^{-8}
$\sigma \varepsilon_w \varepsilon_g A_{wg}$	5.32×10^{-8}

3.2. Reduction model based on sparse identification

A general schematic of sparse identification is provided in Fig. 4. As shown in Eqs. (1)–(3), the CFD model is based on partial differential equations (PDEs) rooted in conservation laws, physical principles, and phenomenological behaviors. Thus, the general form of a nonlinear PDE is formulated as follows:

$$u_t = N(1,\ x,\ u,\ u^2, \ldots,\ u_x,\ u_{xx}, \ldots) \quad (5)$$

where $N(\cdot)$ represents the nonlinear function; u_t and u_x denote partial differentiation in time and space, respectively; and 1 stands for a constant term in the PDE. Since $N(\cdot)$ is usually difficult to determine and only the data generated by the PDE system can be

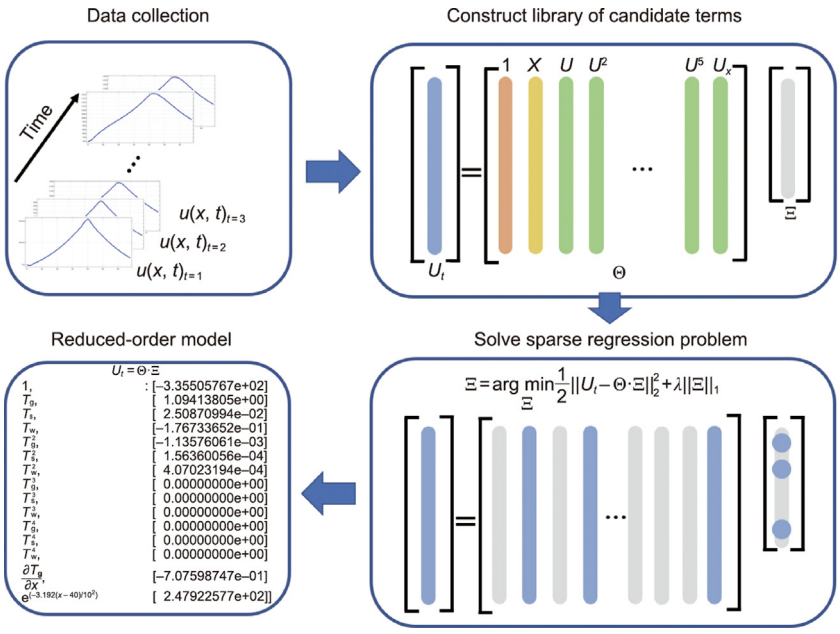

Fig. 4. Schematic of the sparse identification process.

obtained, sparse identification is applied to reconstruct the nonlinear dynamics of $N(\cdot)$, which transforms Eq. (5) into the following form:

$$\hat{u}_t = \sum_{j=1}^{p} \xi_j \theta_j(u) \tag{6}$$

where $\theta_j(u)$ represents a library of nonlinear candidate functions, which may be determined to be polynomials, trigonometric functions, or other forms of functions according to the original dynamics of the system [15,22,26]. j is the index of each nonlinear candidate functions, p is the number of nonlinear candidate functions, ξ_j is a coefficient vector of all candidate terms, and each nonzero entry corresponds to a valid term in the PDE.

To reconstruct $N(\cdot)$ from the data, a series of historical data $U(x, t)$ are collected from the PDE system, and their partial differentiation in time and space, U_t and U_x, are measured or numerically approximated from $U(x, t)$. All data are sampled at several times and arranged into the following matrices:

$$U(x,t) = \begin{bmatrix} u(x_0,t_0) & u(x_0,t_1) & \cdots & u(x_0,t_n) \\ u(x_1,t_0) & u(x_1,t_1) & \cdots & u(x_1,t_n) \\ \vdots & \vdots & \ddots & \vdots \\ u(x_m,t_0) & u(x_m,t_1) & \cdots & u(x_m,t_n) \end{bmatrix} \tag{7}$$

$$U_t(x,t) = \begin{bmatrix} u_t(x_0,t_0) & u_t(x_0,t_1) & \cdots & u_t(x_0,t_n) \\ u_t(x_1,t_0) & u_t(x_1,t_1) & \cdots & u_t(x_1,t_n) \\ \vdots & \vdots & \ddots & \vdots \\ u_t(x_m,t_0) & u_t(x_m,t_1) & \cdots & u_t(x_m,t_n) \end{bmatrix} \tag{8}$$

$$U_x(x,t) = \begin{bmatrix} u_x(x_0,t_0) & u_x(x_0,t_1) & \cdots & u_x(x_0,t_n) \\ u_x(x_1,t_0) & u_x(x_1,t_1) & \cdots & u_x(x_1,t_n) \\ \vdots & \vdots & \ddots & \vdots \\ u_x(x_m,t_0) & u_x(x_m,t_1) & \cdots & u_x(x_m,t_n) \end{bmatrix} \tag{9}$$

Then, a library $\Theta(U)$ consisting of candidate nonlinear functions such as polynomial, trigonometric, and partial differentiation functions in space terms is formulated as follows:

$$\Theta(U) = \left[1, X, U, U^2, U^3, \ldots, \sin(U), \cos(U), \ldots, U_x, U_{xx}, \ldots\right] \tag{10}$$

Similar to Eq. (6), the dynamical system can be approximated as follows:

$$U_t \approx \Theta(U) \cdot \Xi \tag{11}$$

For Eq. (11), it is vital to find a suitable Ξ, which is coefficient vector of each nonlinear candidate function, to perfectly reconstruct $N(\cdot)$ with the function library Θ. Since Θ is over-full, it is reasonable to assume that only a few terms would be chosen to construct $N(\cdot)$ [15,23], which can transform Eq. (11) into a sparse regression problem:

$$\Xi = \arg\min_{\Xi} \frac{1}{2} \| U_t - \Theta \cdot \Xi \|_2^2 + \lambda \| \Xi \|_1 \tag{12}$$

where λ is a hyper-parameter determining the sparsity in coefficient vector Ξ. The above optimization problem is a typical sparse regression problem and can be solved by the sequentially threshold least squares shown in Algorithm 1. Through sparse identification, a few terms that are vital for constructing the original dynamical CFD model are picked up to establish a reduction model whose computational complexity is significantly decreased to meet the demands of real-time computing.

Algorithm 1. Sequentially threshold least squares to solve the sparse regression problem.

Input: Time derivative U_t, library of candidate functions Θ, threshold parameter ε

(1) Initial least squares guess: $\Xi^0 = \Theta^{\dagger} \cdot U_t$

(2) **while** k < max iteration **do**

(3) Find index of small entries: $I_{\text{small}} \leftarrow \text{abs}\left(\Xi^k\right) < \varepsilon$

(4) Set all small entries to zero: $\Xi^k(I_{\text{small}}) = 0$

(5) Get index of big entries: $I_{\text{big}} \leftarrow \text{abs}\left(\Xi^k\right) \geq \varepsilon$

(6) Update Ξ^k: $\Xi^k = \Theta(I_{\text{big}})^{\dagger} \cdot U_t$

(7) $k = k + 1$

(8) **end while**

Output: Sparse coefficient vectors Ξ

3.3. Multi-objective adaptive optimization model predictive control

With the reduction model obtained, it is possible to satisfy the demand of real-time computing and conduct advanced control strategies. For a rotary kiln, the control objective is to optimize the temperature of the solid, T_s, in the reaction zone, which is generally done by manipulating the coal consumption m_{coal} and the movement speed of the solid v_s. Since the national goal of achieving a carbon peak and carbon neutrality has led to new demands on the zinc smelting industry, such as maintaining a high profit while ensuring low resource consumption and green production in process control, traditional stability control has gradually revealed its limitations and disadvantages. Therefore, an MAO-MPC method that includes RTO and MPC layers is proposed in this paper. The structure of the proposed MAO-MPC method is provided in Fig. 5.

3.3.1. Model predictive control

In the MPC layer, the goal is to find a suitable control signal $u(t)$ through online optimization so that the output of the system tracks the reference trajectory $r(t)$ received from the RTO layer as closely as possible. In this paper, given the prediction and control horizons T_p and T_c, the optimization problem can be formulated as follows:

$$\begin{aligned}&\min_{\boldsymbol{U}(t)} \boldsymbol{J}(t) = \min_{\boldsymbol{U}(t)} \left[\boldsymbol{R}(t) - \hat{\boldsymbol{Y}}(t)\right]^{\mathrm{T}} a \left[\boldsymbol{R}(t) - \hat{\boldsymbol{Y}}(t)\right] + \Delta \boldsymbol{U}(t)^{\mathrm{T}} b \Delta \boldsymbol{U}(t)\\ &\text{Subject to}\\ &\hat{y}(t) = f_d(v_s, m_{coal})\\ &|\Delta u(t)| \le \Delta u_{max}\\ &u_{min} \le u(t) \le u_{max}\\ &\hat{y}_{min} \le \hat{y}(t) \le \hat{y}_{max}\end{aligned} \tag{13}$$

where a and b are weight parameters; $\boldsymbol{R}(t) = [r(t+1), r(t+2), \ldots, r(t+T_p)]$ is the reference output; $\hat{\boldsymbol{Y}}(t) = [\hat{y}(t+1), \hat{y}(t+2), \ldots, \hat{y}(t+T_p)]$ is the predictive output; $\boldsymbol{U}(t) = [u(t+1), u(t+2), \ldots, u(t+T_c)]$ is the optimal control input; $\Delta \boldsymbol{U}(t) = [\Delta u(t+1), \Delta u(t+2), \ldots, \Delta u(t+T_c)]$ represents incremental control moves;

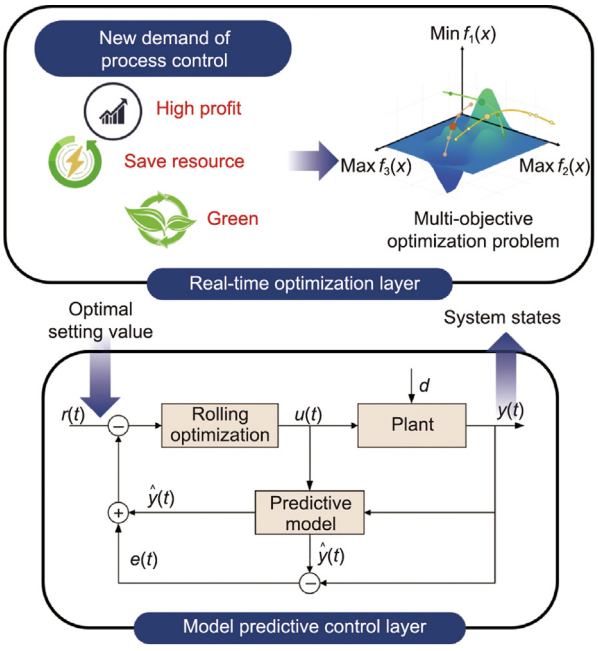

Fig. 5. Schematic of the proposed MAO-MPC method.

and $f_d(\cdot)$ is a dynamical model of the solid temperature, which can be obtained from the sparse identification-based reduction model.

For the optimization problem in Eq. (13), the gradient descent (GD) method is suitable, since all functions are continuous and derivable. More specifically, the expression of the GD method is formulated as follows:

$$\boldsymbol{U}_{k+1}(t) = \boldsymbol{U}_k(t) + \Delta \boldsymbol{U}_k(t) \tag{14}$$

$$\Delta \boldsymbol{U}_k(t) = \eta_1 \left[-\frac{\partial \boldsymbol{J}(t)}{\partial \boldsymbol{U}_k(t)}\right] \tag{15}$$

where $\eta_1 > 0$ is the learning rate, and k is the number of iterations. According to Eq. (13), the derivative of the objective function $\boldsymbol{J}(t)$ can be rewritten as follows:

$$\frac{\partial \boldsymbol{J}(t)}{\partial \boldsymbol{U}_k(t)} = -a \left[\frac{\partial \hat{\boldsymbol{Y}}(t)}{\partial \boldsymbol{U}_k(t)}\right]^{\mathrm{T}} \left[\boldsymbol{R}(t) - \hat{\boldsymbol{Y}}(t)\right] + b \Delta \boldsymbol{U}_k(t) \tag{16}$$

Thus, Eq. (15) can be formulated as follows:

$$\begin{aligned}\Delta \boldsymbol{U}_k(t) &= \eta_1 \left\{ a \left[\frac{\partial \hat{\boldsymbol{Y}}(t)}{\partial \boldsymbol{U}_k(t)}\right]^{\mathrm{T}} \left[\boldsymbol{R}(t) - \hat{\boldsymbol{Y}}(t)\right] - b \Delta \boldsymbol{U}_k(t) \right\}\\ &= \frac{1}{1 + \eta_1 b} \eta_1 a \left[\frac{\partial \hat{\boldsymbol{Y}}(t)}{\partial \boldsymbol{U}_k(t)}\right]^{\mathrm{T}} \left[\boldsymbol{R}(t) - \hat{\boldsymbol{Y}}(t)\right]\end{aligned} \tag{17}$$

For the GD method, the constraints can be managed using the projected gradient method, where the optimization variables are projected onto the allowed hyperspace. Since the constraints in the proposed optimization problem are box constraints (constant or linear constraints), Eqs. (14) and (15) can be modified as follows [39]:

$$\boldsymbol{U}_{k+1}(t) = P_1[\boldsymbol{U}_k(t) + \Delta \boldsymbol{U}_k(t)] \tag{18}$$

$$\Delta \boldsymbol{U}_k(t) = P_2 \eta_1 \left[-\frac{\partial \boldsymbol{J}(t)}{\partial \boldsymbol{U}_k(t)}\right] \tag{19}$$

where $P_1^k[\boldsymbol{U}_k(t)]$ and $P_2^k[\Delta \boldsymbol{U}_k(t)]$ is the projection form for the vectors $\boldsymbol{U}_k(t)$ and $\Delta \boldsymbol{U}_k(t)$. For each element in $\boldsymbol{U}_k(t)$ and $\Delta \boldsymbol{U}_k(t)$, its projection form $P_1^k[u_k(t)]$ and $P_2^k[\Delta u_k(t)]$ can be written as follows:

$$\begin{aligned}P_1^k[u_k(t)] &= \min\{u_{max}, \max[u_{min}, u_k(t)]\}\\ &= \begin{cases} u_{max}, & \text{if } u_k(t) > u_{max}\\ u_k(t), & \text{if } u_{min} \le u_k(t) \le u_{max}\\ u_{min}, & \text{if } u_k(t) < u_{min}\end{cases}\end{aligned} \tag{20}$$

$$\begin{aligned}P_2^k[\Delta u_k(t)] &= \min\{\Delta u_{max}, \max[-\Delta u_{max}, \Delta u_k(t)]\}\\ &= \begin{cases} \Delta u_{max}, & \text{if } \Delta u_k(t) > \Delta u_{max}\\ \Delta u_k(t), & \text{if } -\Delta u_{max} \le \Delta u_k(t) \le \Delta u_{max}\\ -\Delta u_{max}, & \text{if } \Delta u_k(t) < -\Delta u_{max}\end{cases}\end{aligned} \tag{21}$$

where u_{max} is the upper bound constraint on $u_k(t)$, u_{min} is the lower bound constraint on $u_k(t)$, and Δu_{max} is the bound of the incremental control input $\Delta u_k(t)$. In regard to the system state constraints, such as dealing with the control input constraints, the projected method will be added to the prediction model to ensure that the constraints are satisfied. To speed up the optimization process, we propose an improved adaptive GD method that uses a natural logarithm to decay the learning rate; this makes it possible to accelerate the convergence speed of the proposed method:

$$\eta_1^{k+1} = \eta_1^k \mathrm{e}^{-\omega k} \tag{22}$$

where ω is the decay rate of each iteration.

By solving the optimization problem, the optimal control input sequences $u(t)$ can be obtained. Then, the first element of $u(t)$ is

applied as the control signal in the system to make sure that the output of the system can track the reference trajectory, ensuring that the rotary kiln is operating in the optimal state.

3.3.2. Real-time optimization

In the RTO layer, the essential goal is to design an appropriate multi-objective optimization problem based on several new demands on process control. With the solution of the designed optimization problem, an optimal-setting value can be obtained, which ensures that the process works in the optimal state. Meanwhile, the system's real-time states are continuously fed into the RTO layer, promptly updating the optimal-setting value. For a rotary kiln, two aspects are taken into consideration to formulate the multi-objectives optimization problem: coal consumption and product quality. To better evaluate the performance of the production process from these two aspects, we define a cost function as follows:

$$C = C_{\text{Material}} + C_{\text{Production}} \tag{23}$$

where C_{Material} represents the material cost, which is mainly that of coal consumption. This is formulated as follows:

$$C_{\text{Material}} = \alpha \cdot m_{\text{coal}} \tag{24}$$

where α is the coal selling price. $C_{\text{Production}}$ denotes the production cost, which is strongly related to product quality, as better quality can reduce the reproduction number. According to the previous analysis of the zinc oxide rotary kiln, the kiln's function is to improve the zinc recycling rate in useless slag in order to enhance resource utilization. It is clear that the zinc recycling rate depends on the solid temperature in the reaction zone, since a higher temperature can speed up the reaction rate to produce more zinc. Based on this analysis, $C_{\text{Production}}$ is formulated as follows:

$$C_{\text{Production}} = \beta \cdot \mathrm{e}^{-\tau T_{\text{s}}} \tag{25}$$

where β is the cost of reproduction and τ is a hyper-parameter measuring the impact of product quality on production cost. Therefore, the goal of the RTO layer is to minimize the spending cost during the production process, and its optimization problem is designed as follows:

$$\begin{aligned} &\min_{T_{\text{s}}^*} C = \min_{T_{\text{s}}^*} \alpha \cdot m_{\text{coal}} + \beta \cdot \mathrm{e}^{-\tau T_{\text{s}}} \\ &\text{Subject to} \\ &T_{\text{s}}^* = f_{\text{s}}(v_{\text{s}}, m_{\text{coal}}) \\ &v_{\min} \le v_{\text{s}} \le v_{\max} \\ &m_{\min} \le m_{\text{coal}} \le m_{\max} \end{aligned} \tag{26}$$

where v_{s} is the movement speed of solids in the rotary kiln, and $f_{\text{s}}(\cdot)$ represents the steady-state model of the solid temperature, which is obtained from the reduction model. Through the GD method, the optimization problem in Eq. (26) is solved and the optimal-setting value is sent to the MPC layer to improve the performance of the rotary kiln.

4. Experiment

In this section, a series of experiments are designed to demonstrate the strength of the proposed method. The performance is measured using the mean absolute percentage error (MAPE), root mean-square error (RMSE), and average change ($\overline{\Delta u}$) in the manipulated variable, which are defined as follows:

$$\text{MAPE} = \frac{1}{N}\sum_{i=1}^{N}\left|\frac{y_i - \hat{y}_i}{y_i}\right| \times 100\% \tag{27}$$

$$\text{RMSE} = \sqrt{\frac{1}{N}\sum_{i=1}^{N}(y_i - r_i)^2} \tag{28}$$

$$\overline{\Delta u} = \frac{1}{N}\sum_{i=1}^{N}|\Delta u(i)| \tag{29}$$

where r_i represents the reference trajectory, y_i stands for the actual output of the controlled system, $\hat{y}_i$ stands for the output of the prediction model, and $\Delta u(i)$ is the change in the manipulated variable.

4.1. Verification of reduced-order model

At first, whether the reduction model is accurate enough to represent the rotary kiln CFD model determines the control effect on the solid temperature of the reaction zone. Therefore, comparison experiments are conducted to determine whether the sparse identification-based reduction model is reliable. Since the rotary kiln is a typical distributed parameter system, its temperature has a strong relation with time and space; therefore, it is necessary to verify the reduction model from two aspects: a steady state and a dynamic state.

4.1.1. Steady-state verification

The steady state of the rotary kiln CFD model assumes that the system state will not change any further; thus, it mainly focuses on the temperature distribution along the spatial position. The temperature of the solids in the rotary kiln starts at a low point, since the raw material is sent into the kiln without heating. When the raw material gradually moves into the reaction zone, its temperature climbs, finally reaching a maximum somewhere in the reaction zone. Then, the temperature of the solids sharply decreases as they pass through the cooling zone. The result of the comparison experiment is demonstrated in Fig. 6. It can be seen that, regardless of the trend of the temperature distribution curve or the temperature value at each position, the sparse identification-based reduction model is similar to the original CFD model, showing the reliability of the proposed method.

4.1.2. Dynamic-state verification

The dynamic state of the rotary kiln CFD model denotes how the temperature of the solids in the kiln varies with time. For any position inside the rotary kiln, given an initial state, if the control variables remain unchanged and as time passes, the temperature of the solids will gradually approach a steady state. The result of the comparison experiment is demonstrated in Fig. 7. It can be seen that the reduction model can maintain most of the dynamical characteristics of the original CFD model, laying a foundation for process control.

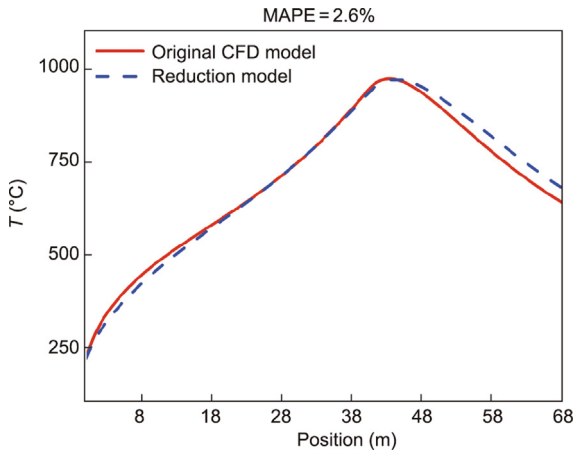

Fig. 6. Result of the comparison experiment on the temperature steady-state distribution of the CFD model and the reduction model.

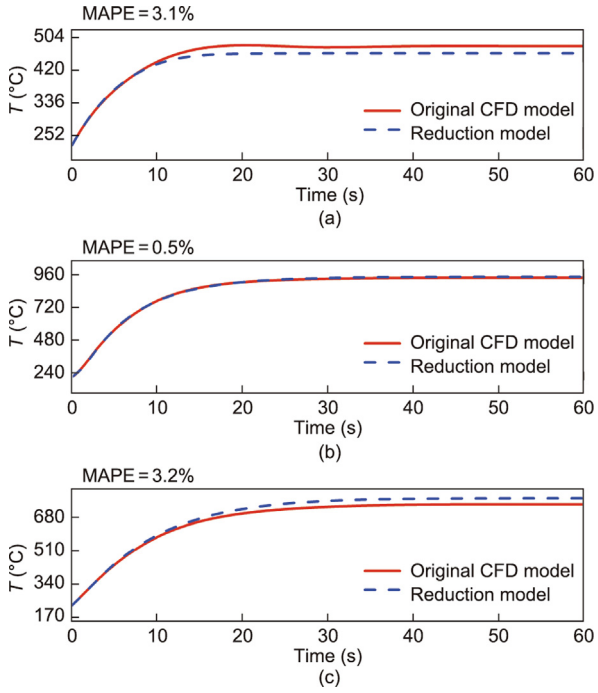

Fig. 7. Result of the comparison experiment on the temperature dynamic-state distribution of the CFD model and the reduction model at different positions: (a) 10 m; (b) 40 m; and (c) 60 m.

Another aspect of verifying the dynamic state of the reduction model is to study whether its dynamic response to probable changes in manipulated variables fits the principle of the zinc oxide rotary kiln. According to field workers' experience, the coal consumption m_{coal} and the movement speed of the solids v_s have a great impact on the temperature of the solids. Regarding coal consumption, it is obvious that more coal means more heat, leading to an increase in temperature. Regarding the movement speed of the solids, this speed determines the time spent by the solids inside the rotary kiln. The longer the solids stay inside the kiln, the higher their temperature will be. In this experiment, a step change in the manipulated variables occurs at some timepoint in order to study the dynamic response of the proposed reduction model. The results are shown in Fig. 8. It can be seen that the dynamic response of the proposed reduction model perfectly fits the principle of the rotary kiln, compared with the original CFD model. According to these verification experiments, the proposed reduction model is demonstrated to be effective, and it can replace the original model to meet the real-time demand for optimal control.

4.2. The control effect on a rotary kiln

In this section, the control effect of the proposed optimal control method is compared with two control schemes that come from field work: ① maintaining the temperature of the tail of the rotary kiln at 600–700 °C; and ② maintaining the temperature of the reaction zone of the rotary kiln at 1000–1200 °C. Both comparison control methods are based on an MPC whose prediction model is the proposed reduction model. During the experiment, the setting values coming from workers' experience are 670 and 1100 °C, respectively. The hyper-parameters for the proposed optimization MPC method are $a = 1$, $b = 1$, $\alpha = 0.035$, $\beta = 4.8$, $\tau = 3.5 \times 10^{-3}$; the prediction horizon is $T_p = 2$; and the control horizon is $T_c = 1$. The control results for all the methods are provided in Fig. 9 and Table 3.

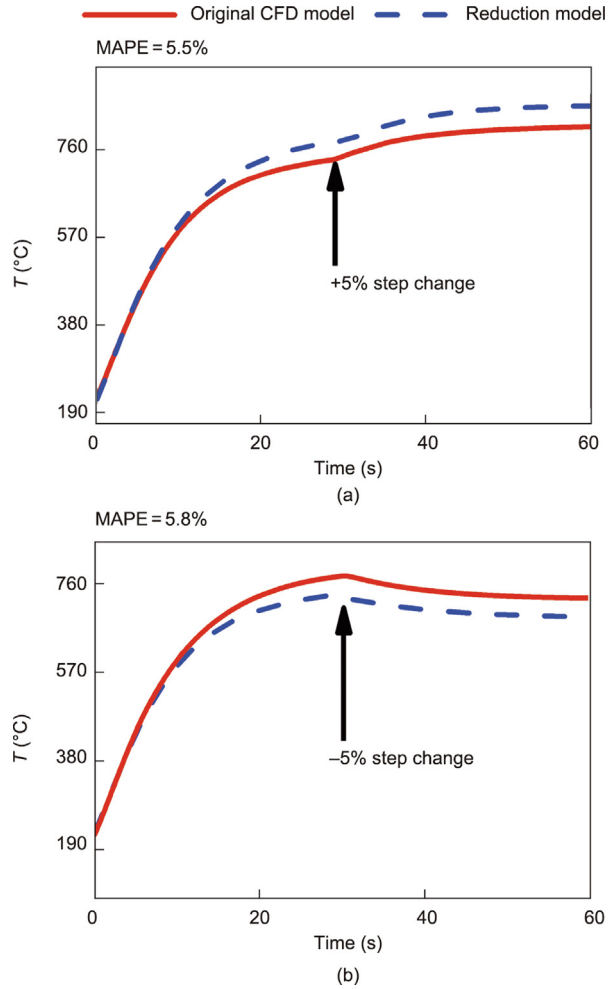

Fig. 8. Results of the comparison experiment on the dynamic response to a step change in the manipulated variables: (a) +5% step change; and (b) −5% step change.

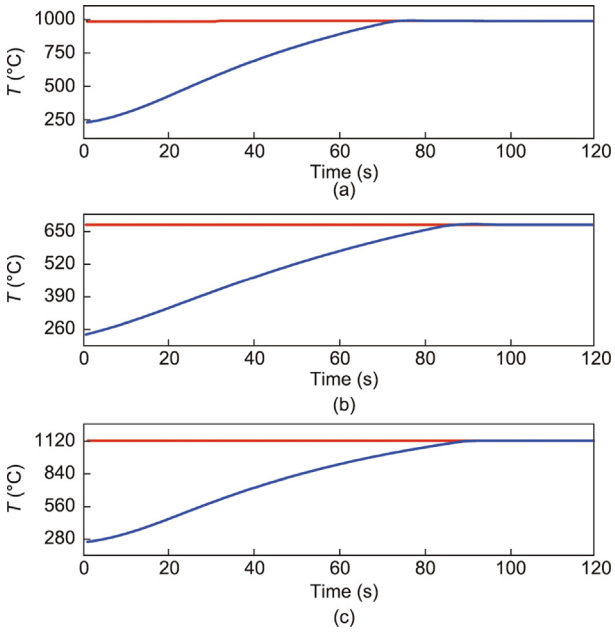

Fig. 9. Control results for the temperature of the rotary kiln: (a) MAO-MPC; (b) MPC (tail of rotary kiln); and (c) MPC (reaction zone of rotary kiln).

Table 3
A comparison of all the control methods.

Method	RMSE	$\overline{\Delta u}$	Coal consumption	Production cost
MPC (tail)	0.747	0.062	5.572	0.384
MPC (reaction zone)	0.874	**0.046**	5.896	0.394
MAO-MPC	**0.497**	0.077	**5.331**	**0.379**

The minimum values of each method are in bold.

From Fig. 9 and Table 3, it can be seen that all the methods can perfectly achieve stability control of the temperature-setting values. However, the overall goal of achieving a carbon peak and carbon neutrality requires higher standards, such as cutting coal consumption. The two comparison methods cannot adjust the temperature-setting value according to the operation states of the rotary kiln, resulting in greater consumption of coal and emissions of greenhouse or polluted gases. The proposed optimal control method designs a multi-objective optimization problem in the RTO layer, which takes the new control demands into consideration and can promptly determine the optimal temperature-setting value for the rotary kiln. Therefore, the proposed method not only keeps the rotary kiln stable but also achieves optimal economic performance and reduces coal consumption.

To compare the time cost for each method, a comparison experiment on the time spent was conducted, as shown in Fig. 10. It was found that the time spent by the proposed method is strongly related to the frequency of the optimization of the setting value, since every optimization process requires solving the steady-state model of the rotary kiln with the help of the ROM. The more frequently the optimization process is conducted, the more time it will take. Moreover, the control effect may not always improve with a higher frequency of optimizing the setting value, since a rotary kiln is a slow change process, so the optimal-setting value remains unchanged for a while. Accordingly, the time required by the proposed method depends on the frequency of optimizing the setting value, which can be determined through the demands of practical application

5. Conclusions

In this work, to meet the new demand for process control in zinc oxide rotary kilns, we proposed a novel model reduction method and two-layered optimal control framework. First, based on sparse identification, the rotary kiln CFD dynamic model was simplified to satisfy real-time computing. Then, the proposed two-layered optimal control method was designed. In the RTO layer, an optimization problem with the goal of achieving optimal process operation performance is set up. By solving the optimization problem in real time, an optimal setting value can be sent to the MPC layer to ensure that the zinc oxide rotary kiln is always working in an optimal state. Several experiments demonstrated that the proposed method can achieve better control performance for a rotary kiln and can reduce coal consumption. In the future, the issue of how to improve accuracy of a first-principles model and design the optimization objective function can be studied to further improve the performance of rotary kilns.

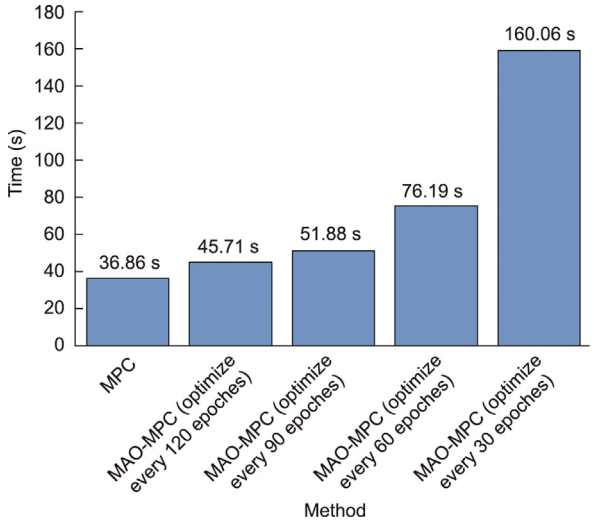

Fig. 10. A comparison of the time required by a simple MPC and the proposed method with different optimization frequencies.

Acknowledgments

This work was supported in part by the National Key Research and Development Program of China (2022YFB3304900), in part by the National Natural Science Foundation of China (61988101, 62073340, and 61860206014), in part by the Major Key Project of Peng Cheng Laboratory (PCL) (PCL2021A09), in part by the Science and Technology Innovation Program of Hunan Province (2022JJ10083, 2021RC3018, and 2021RC4054), and in part by the Innovation-Driven Project of Central South University, China (2019CX020).

Compliance with ethics guidelines

Ke Wei, Keke Huang, Chunhua Yang, and Weihua Gui declare that they have no conflict of interest or financial conflicts to disclose.

References

[1] Zeng Z, Gui W, Chen X, Xie Y, Zhang H, Sun Y. A cell condition-sensitive frequency segmentation method based on the sub-band instantaneous energy spectrum of aluminum electrolysis cell voltage. Engineering 2021;7(9):1282–92.
[2] Dai H, Su Y, Kuang L, Liu J, Gu D, Zou C. Contemplation on China's energy-development strategies and initiatives in the context of its carbon neutrality goal. Engineering 2021;7(12):1684–7.
[3] Cai B, Zhang L, Lei Y, Wang J. A deeper understanding of the CO_2 emission pathway under China's carbon emission peak and carbon neutrality goals. Engineering. In press.
[4] Zhang X, Gao X. The pathway toward carbon neutrality: challenges and countermeasures. Engineering 2022;14:1–2.
[5] Zuo J, Zhong Y, Yang Y, Fu C, He X, Bao B, et al. Analysis of carbon emission, carbon displacement and heterogeneity of Guangdong power industry. Energy Rep 2022;8(Suppl 6):438–50.
[6] Mujumdar KS, Ranade VV. CFD modeling of rotary cement kilns. Asia-Pac J Chem Eng 2008;3(2):106–18.
[7] Li W, Wang D, Chai T. Burning state recognition of rotary kiln using ELMs with heterogeneous features. Neurocomputing 2013;102:144–53.
[8] Chai T, Ding J. Smart and optimal manufacturing for process industry. Strateg Study Chin Acad Eng 2018;20(4):51–8. Chinese.
[9] Boateng AA, Barr PV. A thermal model for the rotary kiln including heat transfer within the bed. Int J Heat Mass Transf 1996;39(10):2131–47.
[10] Wang Z, Wang TR, Yuan M, Wang H. Dynamic model for simulation and control of cement rotary kilns. J Syst Simul 2008;20(19):5131–5.
[11] Hanein T, Glasser FP, Bannerman MN. One-dimensional steady-state thermal model for rotary kilns used in the manufacture of cement. Adv Appl Ceramics 2017;116(4):207–15.

[12] Rodrigues DCQ, Soares Jr AP, Costa Jr EF, Costa AOS. Dynamic analysis of the temperature and the concentration profiles of an industrial rotary kiln used in clinker production. An Acad Bras Ciênc 2017;89(4):3123–36.
[13] Witt PJ, Sinnott MD, Cleary PW, Schwarz MP. A hierarchical simulation methodology for rotary kilns including granular flow and heat transfer. Miner Eng 2018;119:244–62.
[14] Ditaranto M, Bakken J. Study of a full scale oxy-fuel cement rotary kiln. Int J Greenh Gas Control 2019;83:166–75.
[15] Narasingam A, Sang-Il KJ. Data-driven identification of interpretable reduced-order models using sparse regression. Comput Chem Eng 2018;119:101–11.
[16] Pitchaiah S, Armaou A. Output feedback control of dissipative PDE systems with partial sensor information based on adaptive model reduction. AIChE J 2013;59(3):747–60.
[17] Benner P, Gugercin S, Willcox K. A survey of projection-based model reduction methods for parametric dynamical systems. SIAM Rev 2015;57(4):483–531.
[18] Yang M, Armaou A. Synthesis of equation-free control structures for dissipative distributed parameter systems using proper orthogonal decomposition and discrete empirical interpolation methods. Ind Eng Chem Res 2017;56(36):10110–22.
[19] Van Overschee P, De Moor B. N4SID: subspace algorithms for the identification of combined deterministic-stochastic systems. Automatica 1994;30(1):75–93.
[20] Viberg M. Subspace-based methods for the identification of linear time-invariant systems. Automatica 1995;31(12):1835–51.
[21] Qin SJ. An overview of subspace identification. Comput Chem Eng 2006;30(10–12):1502–13.
[22] Brunton SL, Proctor JL, Kutz JN. Discovering governing equations from data by sparse identification of nonlinear dynamical systems. Proc Natl Acad Sci USA 2016;113(15):3932–7.
[23] Rudy SH, Brunton SL, Proctor JL, Kutz JN. Data-driven discovery of partial differential equations. Sci Adv 2017;3(4):1602614.
[24] Huang K, Tao Z, Wang C, Guo T, Yang C, Gui W. Cloud-edge collaborative method for industrial process monitoring based on error-triggered dictionary learning. IEEE Trans Ind Inform 2022;18(12):8957–66.
[25] Kaiser E, Kutz JN, Brunton SL. Sparse identification of nonlinear dynamics for model predictive control in the low-data limit. Proc R Soc A 2018;474 (2219):20180335.
[26] Bhadriraju B, Bangi MSF, Narasingam A, Sang-Il KJ. Operable adaptive sparse identification of systems: application to chemical processes. AIChE J 2020;66 (11):e16980.
[27] Li J, Sun G, Zhao G, Lehman LH. Robust low-rank discovery of data-driven partial differential equations. Proc AAAI Conf Artif Intell 2020;34(1):767–74.
[28] Han H, Qiao J. Nonlinear model-predictive control for industrial processes: an application to wastewater treatment process. IEEE Trans Ind Electron 2014;61 (4):1970–82.
[29] Han HG, Zhang L, Hou Y, Qiao JF. Nonlinear model predictive control based on a self-organizing recurrent neural network. IEEE Trans Neural Netw Learn Syst 2016;27(2):402–15.
[30] Wang G, Jia QS, Qiao J, Bi J, Zhou MC. Deep learning-based model predictive control for continuous stirred-tank reactor system. IEEE Trans Neural Netw Learn Syst 2021;32(8):3643–52.
[31] Teja R, Sridhar P, Guruprasath M. Control and optimization of a triple string rotary cement kiln using model predictive control. IFAC-PapersOnLine 2016;49(1):748–53.
[32] Wurzinger A, Leibinger H, Jakubek S, Kozek M. Data driven modeling and nonlinear model predictive control design for a rotary cement kiln. IFAC-PapersOnLine 2019;52(16):759–64.
[33] Stadler KS, Poland J, Gallestey E. Model predictive control of a rotary cement kiln. Control Eng Pract 2011;19(1):1–9.
[34] Machalek D, Powell KM. Model predictive control of a rotary kiln for fast electric demand response. Miner Eng 2019;144:106021.
[35] Rawlings JB, Amrit R. Optimizing process economic performance using model predictive control. In: Magni L, Raimondo DM, Allgöwer F, editors. Nonlinear model predictive control: towards new challenging applications. Heidelberg: Springer, Berlin; 2009. p. 119–38.
[36] Wu Q, Du W, Nagy Z. Steady-state target calculation integrating economic optimization for constrained model predictive control. Comput Chem Eng 2021;145:107145.
[37] Fan X, Li J, Chen X, Wang Y, Gan M. Temperature field simulation model for rotary kiln of iron ore oxidized pellet. J Iron Steel Res Int 2013;20(4):16–9.
[38] Li SQ, Ma LB, Wan W, Yao Q. A mathematical model of heat transfer in a rotary kiln thermo-reactor. Chem Eng Technol 2005;28(12):1480–9.
[39] Viljoen JH, Muller CJ, Craig IK. Hybrid nonlinear model predictive control of a cooling water network. Control Eng Pract 2020;97:104319.